Bone 120 (2019) 347–353

Contents lists available at ScienceDirect

Bone

journal homepage: www.elsevier.com/locate/bone

Full Length Article

Bone remodeling following MR-guided focused ultrasound: Evaluation with HR-pQCT and FTIR

Matthew D. Bucknor*, Harsh Goel, Courtney Pasco, Andrew E. Horvai, Galateia J. Kazakia

Department of Radiology and Biomedical Imaging, University of California San Francisco, 185 Berry Street, Suite 350, San Francisco, CA 94107-5705, United States

ARTICLE INFO

Keywords:
Magnetic resonance-guided focused ultrasound (MRgFUS)
High intensity focused ultrasound (HIFU)
Ablation
Fourier transform infrared spectroscopy (FTIR)
High resolution peripheral quantitative computed tomography

ABSTRACT

Magnetic resonance-guided focused ultrasound (MRgFUS) is a novel non-invasive ablation technique that uses focused sound energy to destroy focal tumors, primarily via heat deposition. It is widely used for palliation of pain from bone metastases and has also recently gained popularity as a technique for ablation of benign bone tumors and facet degenerative joint disease (rhizotomy). Clinically, in a subset of patients who have undergone MRgFUS of bone, a variety of treatment responses have been noted on follow-up imaging, including focal sclerosis within the target lesion or more exuberant proliferative changes associated with the periosteum.

In this study, high resolution peripheral quantitative CT (HR-pQCT) was used to evaluate remodeling of bone following ablation in a swine model of MRgFUS and compared to samples from a control, non-treated femur. Within each treated femur, two lesions were created: a higher energy focused ultrasound dose was used for one lesion compared to a lower energy dose for the second lesion. Exuberant, extra-cortical bone formation was detected at the higher energy ablation zones, with volumes ranging from 340 mm^3 to 1040 mm^3. More subtle endosteal and cortical changes were detected in the lower energy ablation zones, however cortical thickness was significantly increased at these sites compared to control bone. For both high and low energy lesions, lower bone mineral density and tissue mineral density was noted in treated regions compared to control regions, consistent with the formation of newly mineralized tissue.

Following HR-pQCT analysis, Fourier transform infrared (FTIR) spectroscopy was subsequently used to detect biochemical changes associated with remodeling of bone following MRgFUS, and compared to samples from the control, non-treated femur. Findings were compared with histopathologic examination following hematoxylin-eosin staining. FTIR analysis demonstrated lower mineral/phosphate ratio and increased crystallinity compared to the control samples ($p = 0.013$). Histopathologic review demonstrated associated areas of endosteal inflammation, scarring, fat necrosis, and new extra-cortical bone formation associated with the ablations. Overall, these findings provide novel characterization of new bone formation following MRgFUS ablation.

1. Introduction

Magnetic resonance-guided focused ultrasound (MRgFUS, also known as high intensity focused ultrasound or HIFU) is a completely noninvasive ablation technique that can be used to focally ablate osseous lesions. It has proven highly effective in palliation of painful bone metastases, but has also shown promise for a variety of other indications, including ablation of osteoid osteomas, facet rhizotomy for treatment of lower back pain, as well as ablation of additional symptomatic benign osseous lesions [1–7]. While its efficacy in these clinical scenarios has been demonstrated, the patterns of bone remodeling following MRgFUS are less well understood. Anecdotally, there has been evidence of focal sclerosis or new bone formation associated with treatment of osseous metastases [7]. Prior basic science studies have also revealed evidence of prominent subperiosteal new bone formation following MRgFUS of bone, with evidence that the pattern of bone remodeling is influenced by technical parameters of the ablation including, for example, acoustic power and duration [8–10]. These findings resemble changes in bone known to be associated with low intensity pulsed ultrasound (LIPUS) [11–13]. However, quantification of structural and compositional changes which occur in and adjacent to bone following higher energy MRgFUS are, otherwise, not well understood. An improved understanding of structural and compositional changes in bone following MRgFUS is critical for optimizing existing treatment indications and providing technical guidance moving forward as the number of potential MRgFUS applications rapidly

* Corresponding author.
E-mail address: matthew.bucknor@ucsf.edu (M.D. Bucknor).

https://doi.org/10.1016/j.bone.2018.11.009
Received 10 September 2018; Received in revised form 8 November 2018; Accepted 12 November 2018
Available online 16 November 2018

increases.

High-resolution peripheral quantitative computed tomography (HR-pQCT) allows for quantitative analysis of bone density, geometry, and microstructure within both trabecular and cortical compartments [14–17]. Fourier transform infrared (FTIR) spectroscopy is a complimentary technique which provides a method for examining tissue quality and composition by measuring molecular bond vibration frequencies to provide information on the structure and environment of the mineral phase of the organic and inorganic components of bone [18–20]. The goal of the current work was to quantify structural and compositional changes in bone quality following MRgFUS with HR-pQCT and FTIR. Specifically, we applied HR-pQCT and FTIR techniques to analyze samples obtained from the proximal and distal femur, at 3 weeks and 6 weeks following ablation, in a swine model of MRgFUS. Our results show that the MRgFUS can produce regions of new bone growth which demonstrate increased cortical thickness, lower bone density, and increased maturity relative to normal bone.

2. Materials and methods

The procedures of MRgFUS ablation have been previously reported [9] and are summarized here. Samples from the eight animals described in that previous study were also used for the new quantitative analyses performed in the current study.

2.1. MRgFUS ablation procedure

Experimental procedures received approval from the local Institutional Animal Care and Use Committee (IACUC). Eight healthy female farm pigs (body mass = 31.0 ± 1.7 kg) (Pork Power Farms, Turlock, CA, USA) were anesthetized with standard techniques, as previously described [9]. An MRgHIFU system (ExAblate2000, Insightec, Haifa, Israel) with a phased array transducer of 208 elements embedded in an MR scanner table was used to create the bone ablations. The table was connected to an MRI scanner (Discovery MR750w 3 T, GE, Milwaukee, WI, USA). In each animal, the skin above the targeted areas in the right femur was shaved, cleaned, and examined for skin defects or scars which might impede the propagation of acoustic energy. Each pig was placed onto the scanner table in the right lateral decubitus position, inside a shallow bath filled with degassed water. A three-plane localizer verified adequate position, followed by treatment planning sequences (non-enhanced T2-weighted fat saturated images). The skin surface and cortical surface of the bone were manually segmented. An ovoid ablation (2 cm in craniocaudal dimension) was prescribed on the MR planning images along the lateral margin of the right femur at the distal femora, metadiaphysis. The metadiaphysis was chosen to allow adequate spacing for two target regions within a single femur. A low-energy test sonication was performed in the adjacent soft tissues to confirm system precision.

Each focal spot sonication lasted 20 s in duration and was performed at a frequency of 1.05 MHz, with a subsequent cooling duration of 25 s. The average energy for the focal spots to compose proximal ablations ranged from 300 to 360 J and from 360 to 440 J for distal ablations. Acoustic power was used to vary energy dose with a goal of creating a 7–10 °C difference between the proximal (desired temperature increase to 60 °C) and distal (desired temperature increase to 67–70 °C) ablations. Increases in temperature were monitored using real-time MR thermometry in the soft tissues adjacent to the targeted bone with multiphase, multi-slice echo planar imaging (FOV/slice thickness/TR/TE/flip angle/echo train length/matrix/BW = 28 cm/3.6 mm/210 ms/18.3 ms/35/12/144 × 144/35 kHz). 3D spoiled gradient echo images (FOV/slice thickness/TR/TE/flip angle = 44 × 44 cm/3.8 mm/4.3 ms/2 ms/15) were subsequently obtained after contrast media administration (0.15 mmol/kg Gd-DTPA) to demonstrate the regions of the ablations.

2.2. HR-pQCT imaging

At 3 and 6 weeks following, MRgFUS, eight treated femurs (2 treated and 2 control at each of 3 and 6 weeks) were dissected from cadaver specimens with an approximately 3–5 cm surrounding cuff of intact muscle and then scanned within 60 min of dissection using a clinical HR-pQCT system (XtremeCT, Scanco Medical AG, Brüttisellen, Switzerland). For tomography, 1000 projections were acquired over 180° with a 200 ms integration time at each angular position, with 60 kVp source potential and 900 mA current. The 12.6 cm FOV was reconstructed across a 3072 × 3072 matrix using a modified Feldkamp algorithm, yielding isotropic 41 μm voxels. The reconstructed linear attenuation values were converted to hydroxyapatite (HA) mineral density values based on a separate scan of a density calibration phantom.

HR-pQCT image processing was performed in Image Processing Language (IPL, Scanco Medical AG). Reconstructed images were binarized to distinguish bone from background using an adaptive iterative threshold selection algorithm. The regions of treatment and contralateral control regions were identified using reference MR procedural imaging. The eight treated specimens were then analyzed. Structural parameters were calculated from the binarized volumes using direct three-dimensional methods [21]. For the high energy ablation sites, new bone formation was manually delineated from native bone (Fig. 1). Within each new bone formation volume, bone volume and bone volume as a proportion of total volume or bone volume fraction (BV/TV) was measured by direct voxel counting of bone and background phases. Volumetric bone mineral density (BMD) was calculated by taking the mean HA density for all voxels within each volume of interest. Similarly, tissue mineral density (TMD) was calculated by taking the mean density for all voxels within each volume of interest, excluding non-osseous regions. Values for the newly formed bone at the high energy lesions were compared to those for the native cortex opposite the ablated region at the same cross-section. Evaluation of cortical thickness was deferred for the high energy lesions, as it was difficult to precisely define this specific dimension in the areas of florid new bone growth. For the low energy ablation sites, no such large foci of extra-cortical new bone were detected; rather, more subtle endosteal changes and

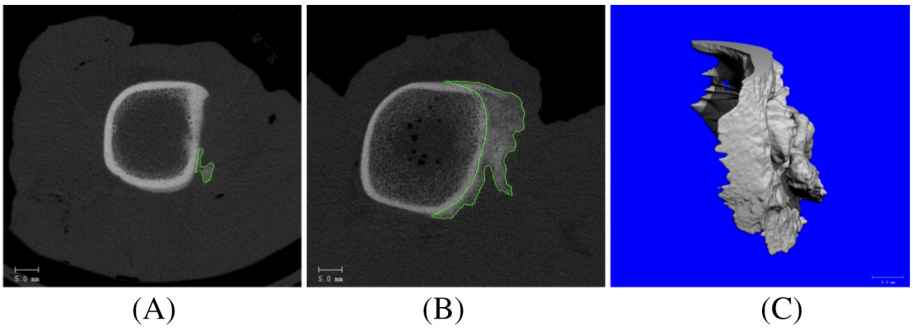

Fig. 1. HR-pQCT images demonstrating segmentation of areas of new bone formation along the cortical margin in regions targeted with MRgFUS ablation at (A) 3 weeks and (B) 6 weeks after the procedure. C) 3D rendering of segmented new bone region in the 6-week sample. These more florid areas of new bone formation were only seen in the regions targeted with relatively higher energies.

changes in cortical thickness were visible on HR-pQCT. To capture these changes, the portion of the cortex within the sonication zone was identified. Cortical thickness (Ct.Th) within this zone was quantified using a 3D sphere filling technique (Laib Hauselmann Ruegsegger Technol Health Care 1998). Volumetric BMD and TMD were calculated as described above. Values for the ablated site were compared to those for native bone from the contralateral control femur at the same anatomic position in the cortex, as an estimate of pre-treatment Ct.Th, BMD, and TMD.

2.3. FTIR spectroscopy

FTIR spectroscopy was performed on the new bone formed adjacent to the high energy ablation regions, and compared to data for native bone within the same femoral cross-section. Following HR-pQCT imaging, cross-sectional samples were dissected at the site of the high energy treated specimens, using procedural MR imaging as a measurement reference. Bones were excised, stripped of soft tissue, and fixed in 70% ethanol. Three foci within each new bone region were isolated, as well as 3 foci within the native cortex on the same cross-section, opposite to the ablated region. FTIR was performed only on those high energy sonication zones where new tissue formation was able to be definitively differentiated by eye from the native bone (4 high energy ablation zones × 3 foci in each: n = 12 treated and 12 control FTIR samples) These samples were desiccated through an ethanol series, followed by exposure in a desiccant chamber.

For each of the isolated samples, a 2-mg (approximately 2 mm long) bone segment was isolated and a homogenized powder mixture was created of 1% bone by weight in potassium bromide (KBr; Thermo Electron, Waltham, MA). The powder mixture was compressed using a manual die to create a pellet for FTIR spectroscopy. Spectroscopy was performed on a benchtop interferometer system (Nexus 870, Thermo Electron). Spectra were acquired using 256 scans at a spectral resolution of 4 cm^{-1}. A background scan was recorded immediately after each sample scan to facilitate background correction. After acquisition, the spectra were transferred to chemical imaging software (Isys; Spectral Dimensions, Olney, MD) for analysis. Spectra were baseline-adjusted and the integrated areas of the amide I (1595–1720 cm^{-1}), m1m3 phosphate (PO_4^{3-}, 895–1215 cm^{-1}), and v2 carbonate (CO_3^{2-}, 840–890 cm^{-1}) bands were calculated. Mineral-to-matrix (PO_4^{3-}/amide I), carbonate-to-matrix (CO_3^{2-}/amide I), and carbonate-to-phosphate (CO_3^{2-}/PO_4^{3-}) ratios were calculated from integrated areas of the respective peaks. Carbonate-to-phosphate ratio is a measure of the amount of substitutions (or imperfections) incorporated into the stoichiometric lattice. Additionally, peak heights were measured at specific wave numbers: 1020, 1030, 1112, 1660, and 1690 cm^{-1}. From these, a series of absorbance ratios were calculated to determine additional spectroscopic parameters. The ratio of 1112 to 1030 cm^{-1} represents the ratio of fresh precipitate to phosphate, termed mineral immaturity index. Higher mineral immaturity index indicates more recently deposited mineral. The ratio of 1030 to 1020 cm^{-1} represents the ratio of stoichiometric apatite to nonstoichiometric apatite, a measure of crystallinity. Higher crystallinity indicates larger, more perfect mineral crystals. Finally, the ratio of 1660 to 1690 cm^{-1} represents the proportion of non-reducible to reducible cross-links in the collagen, indicative of collagen maturity.

2.4. Histology

Histological methods and analysis have been previously reported [8]. Samples were obtained from the midcraniocaudal length of each ablation of the dissected specimens, as defined by the area of bone changes on HR-pQCT. A single 1-cm-thick cross-sectional slice was obtained through the bone and adjacent soft tissues from each of the two ablations in each treated limb. Samples were also taken from the contralateral side at the level of the treatments. From each slice, the medial and lateral portions of the specimen were further dissected, fixed in 10% buffered formalin, decalcified in Easy-Cut decal (American Mastertech, Lodi, Calif), processed in an automated tissue processor (Peloris II; Leica Biosystems, Buffalo Grove, Ill), embedded in paraffin, sliced, and stained with hematoxylin-eosin by using conventional techniques. Slides were reviewed by a bone and soft-tissue pathologist with > 10 years of experience.

2.5. Statistical analysis

Means and SDs were calculated for all indices. Two-tailed paired *t*-tests were used to compare means and standard deviations between treated and controlled specimens as well as between 3 and 6 week time points. 95% confidence intervals were calculated for all means. *p*-Values < 0.05 were considered statistically significant. Statistical analyses were performed in JMP (Version 7.0, SAS Institute Inc., Cary, NC) and R (v.2.13.0, http://www.r-project.org/foundation/).

3. Results

3.1. HR-pQCT analysis

Both high energy and low energy sonications were associated with areas of peripheral new bone growth along the cortical margins, which

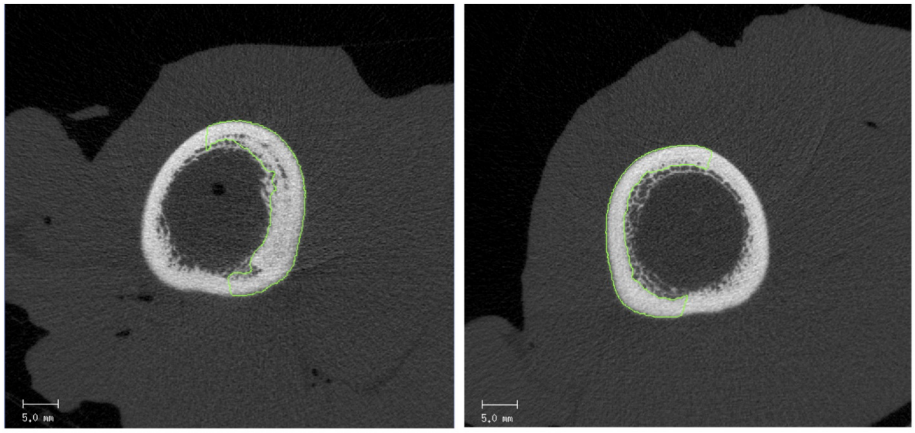

Fig. 2. HR-pQCT image demonstrating changes in bone remodeling along the cortical margin of bone targeted with MRgFUS ablation at 6 weeks following the procedure, including increased cortical thickness in the A) treated femur, compared to the B) control untreated femur from the same animal.

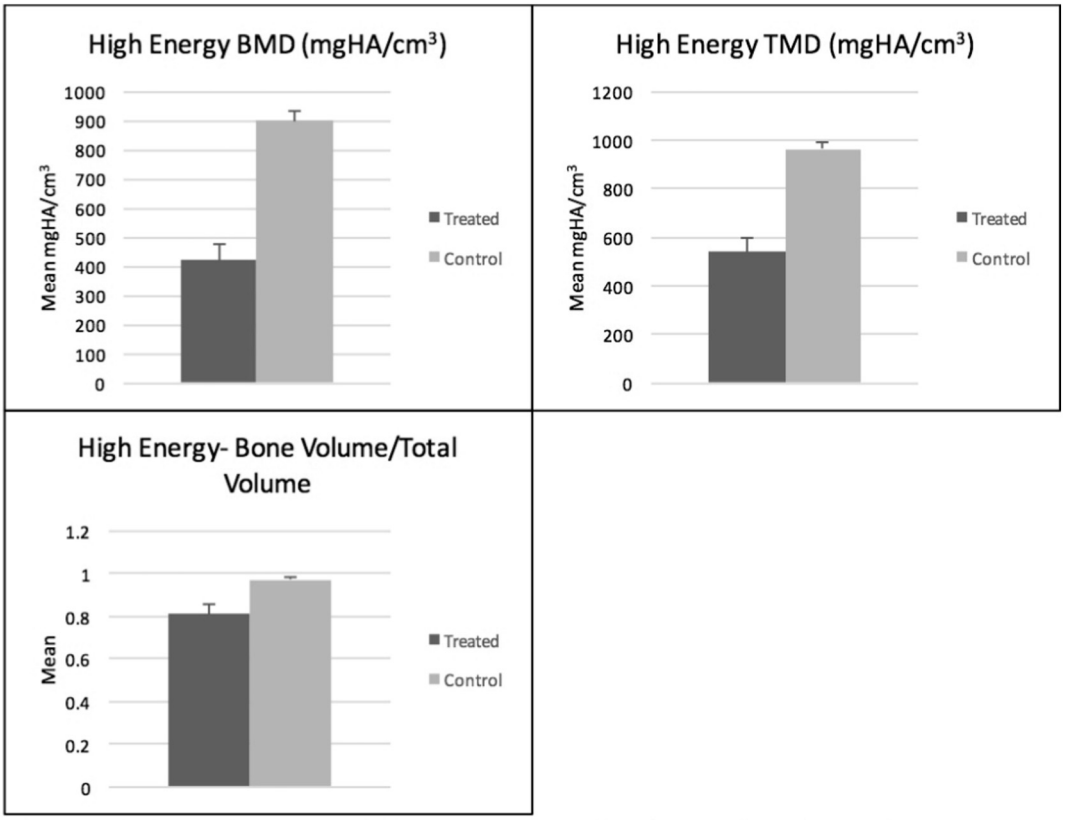

Fig. 3. HR-pQCT analysis of high energy treated and control specimens demonstrate a significantly lower bone mineral density ($p < 0.001$), lower tissue mineral density ($p < 0.001$), and lower bone volume/total volume ($p < 0.001$) in the area of new bone formation at the treated sites, compared to the control regions of bone. Error bars denote 95% confidence intervals.

were not seen in the equivalent control regions of the opposite side of the femur (Figs. 1 and 2). Structural imaging analyses demonstrated significant differences between treated and control specimens for both the high energy and low energy MRgFUS ablations, with regard to the characterization of the regions of new bone growth.

The area of new bone formation in the regions of the high energy ablations was primarily extra-cortical, extending beyond the margin of the native bone, and also subperiosteal. The volume of new bone formed outside of the original cortical margin ranged from 340 mm^3 to 1040 mm^3 (mean ± SD 734 ± 263 mm^3). This new bone region showed lower BMD (421 ± 84 mg/cm^3 vs. 900 ± 46 mg/cm^3, $p < 0.001$) and TMD (540 ± 87 mg/cm^3 vs. 962 ± 38 mg/cm^3, $p < 0.001$) compared to the control regions of the same femur (Fig. 3). The changes in BMD and TMD evolved from 3 to 6 weeks, with progressive increases in BMD, TMD, and BV/TV ratio over this time frame (Fig. 4). Low energy sonications resulted in bone formation at the endosteal boundary of the cortex. These regions similarly demonstrated lower TMD at the treated sites compared to controls (877 ± 2.8 mg/cm^3 vs. 912 ± 2.6 mg/cm^3) (Fig. 5).

3.2. FTIR spectroscopy

FTIR spectroscopy was performed to assess bone quality in bone samples obtained from high energy MRgFUS sonication regions. The analysis showed a significantly lower mineral immaturity index (mean 0.63 ± 0.09 vs. 0.72 ± 0.03, $p = 0.01$) and increased crystallinity (mean 1.05 ± 0.04 vs. 1.01 ± 0.01, $p = 0.01$) in the new bone regions compared to the native bone. Though this is an area of new bone growth, these results suggest increased bone maturity relative to control bone specimens. No other significant differences were observed between the treated and controlled specimens in the FTIR analysis (carbonate/phosphate, mineral/matrix, or crosslink ratio) (Fig. 6).

The differences in mineral immaturity index and crystallinity showed dynamic changes over the 3 and 6 week time points. For example, the differences between treated and controlled mineral immaturity index at 3 weeks (0.49 ± 0.06 vs. 0.71 ± 0.05, $p = 0.11$) were not significant, however, differences between treated and controlled mineral immaturity index at 6 weeks (0.67 ± 0.04 vs. 0.72 ± 0.02, $p = 0.019$) were statistically significant. Similarly, with respect to crystallinity, significant differences were observed between treated (1.04 ± 0.03) and control (1.00 ± 0.008) groups at 6 weeks ($p = 0.034$), while differences between treated and controlled at 3 weeks did not reach significance (1.09 ± 0.05 vs. 1.01 ± 0.01, $p = 0.21$).

3.3. Histology

Histopathologic findings have been previously reported in detail [8]. Briefly, hematoxylin-eosin stained samples taken at 3 weeks demonstrated acute-on-chronic endosteal inflammation with osteonecrosis and bone resorption at the low energy ablations while high energy ablations at 3 weeks demonstrated a similar pattern of endosteal inflammation, with a small area of new extra-cortical bone formation. At 6 weeks, the low energy ablations demonstrated atrophy, scarring, and chronic inflammation with subcortical osteonecrosis and endosteal fat necrosis, while high energy ablations demonstrated those changes along with marked increased extra-cortical new bone formation (Fig. 7). These changes were not seen in the contralateral control femur, which demonstrated normal bone architecture.

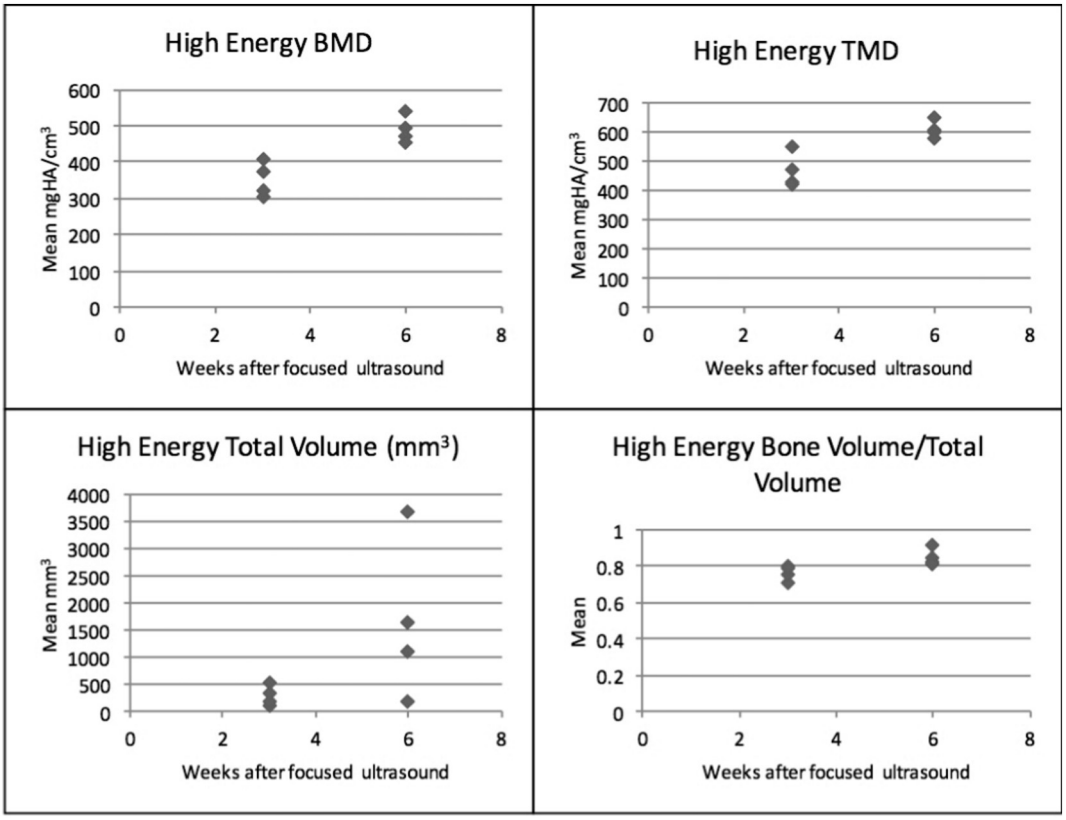

Fig. 4. HR-pQCT analysis of high energy treated samples obtained at 3 and 6 weeks demonstrate significantly increased bone mineral density ($p = 0.002$), tissue mineral density ($p = 0.003$), and Bone Volume/Total Volume ratio ($p = 0.01$) at 6 weeks compared to 3 weeks.

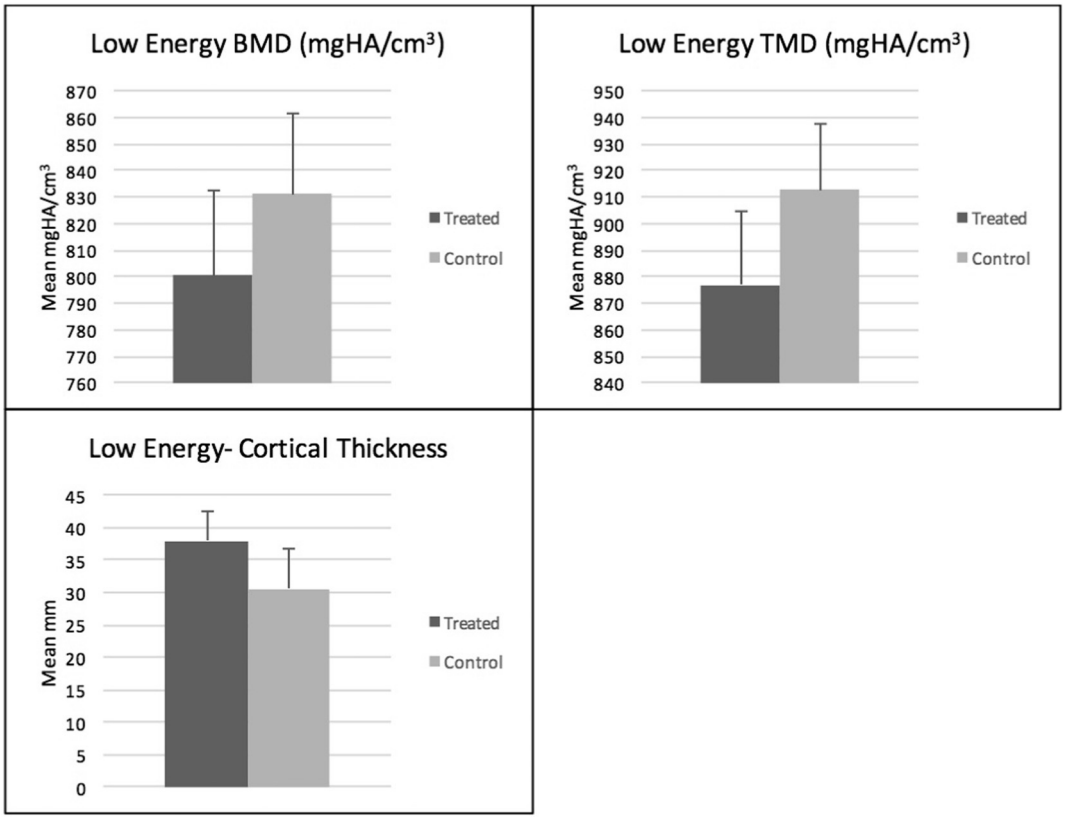

Fig. 5. HR-pQCT analysis of low energy treated and control specimens demonstrate increased cortical thickness ($p = 0.005$) and lower tissue mineral density ($p = 0.04$) at the treated sites compared to the control regions of bone. Differences in bone mineral density did not reach the threshold of statistical significance ($p = 0.09$). Error bars denote 95% confidence intervals.

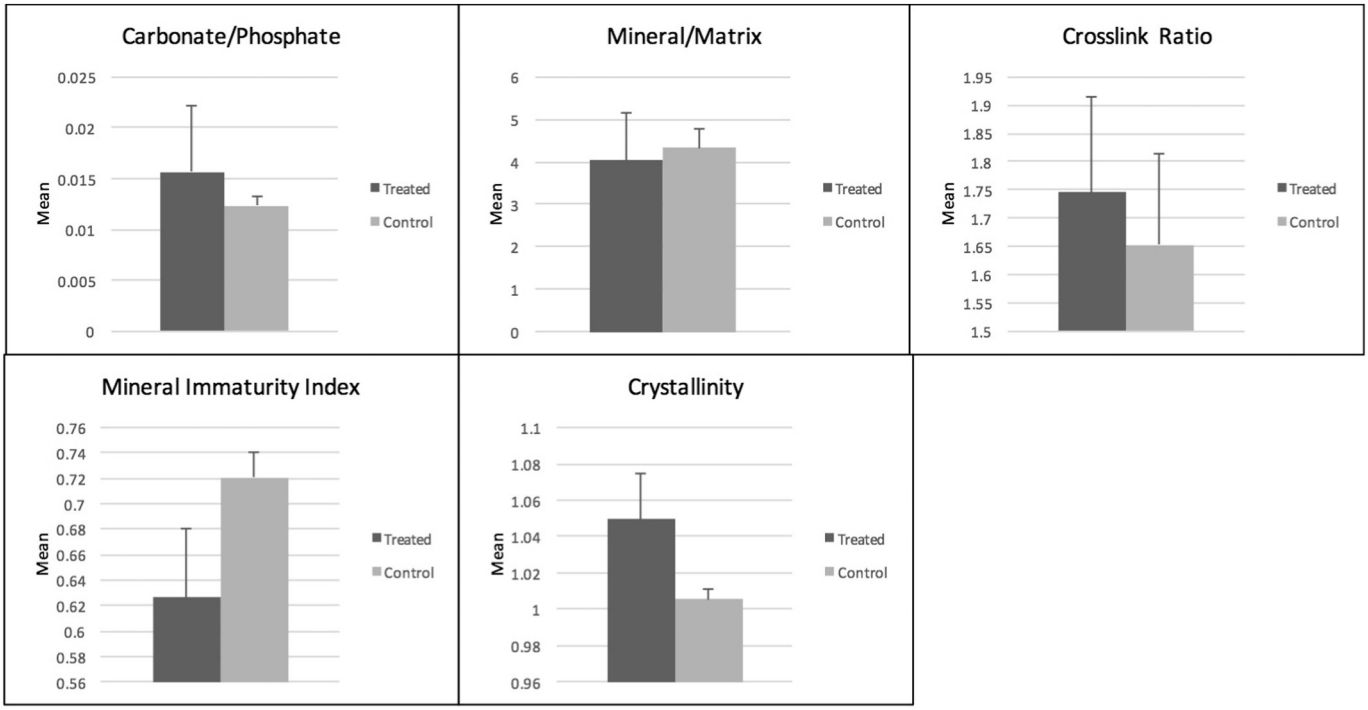

Fig. 6. FTIR analysis of all treated versus control specimens demonstrate a significantly lower Mineral Immaturity Index (mean 0.63 vs. 0.72, $p = 0.01$) and significantly increased Crystallinity (1.05 vs. 1.01, $p = 0.01$) at the treated femoral sites. The remaining FTIR spectroscopic parameters did not show significant differences between the two groups. Error bars denote 95% confidence intervals.

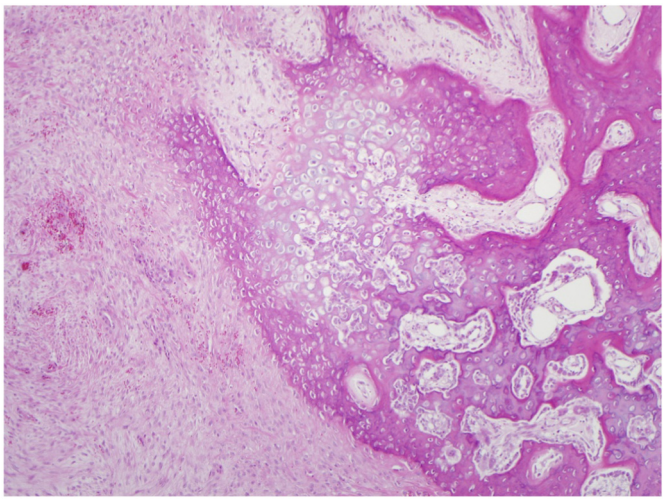

Fig. 7. Hematoxylin-eosin-stained slice obtained from a high energy ablation site at 6 weeks after MRgFUS demonstrating exuberant areas of extra-cortical subperiosteal new bone formation. (Original magnification, ×100).

4. Discussion

This study provides a more detailed characterization of areas of new bone formation following MRgFUS than has been previously reported. HR-pQCT images demonstrated extra-cortical new bone formation along the margin of bone at 3 weeks following MRgFUS, which increased in overall volume at 6 weeks. These changes in bone volume were associated with dramatic morphological changes and alterations in microstructure, with relatively lower TMD and BMD noted in the treated regions on HR-pQCT analysis. HR-pQCT analyses were dynamic with significantly increasing TMD and BMD at 6 weeks compared to 3 weeks. The largest foci of new bone formation were noted at the sites targeted with high energy sonications, suggesting a dose dependent relationship.

Quantitative FTIR analysis indicate this bone remodeling to be a rapidly evolving process with changes in the Mineral Immaturity Index and Crystallinity suggesting increased maturity within the areas of new bone formation relative to native bone. This result is unexpected, particularly given the lower TMD and BMD within these foci of new bone, and thus emphasizing the need for additional studies of varied duration and broader range of MRgFUS energies to better understand the patterns of remodeling of bone tissue quality following MRgFUS.

While LIPUS has been shown across multiple studies to stimulate new bone formation following fracture through recruitment of local and circulating osteogenic progenitors and acceleration of all stages of the fracture repair process, the precise mechanism of new bone formation following MRgFUS remains poorly understood [13,22]. Possible etiologies include stimulation of repair mechanisms following injury and/or mechanical effects related to ultrasound properties. However, further studies are needed to better understand the evolving patterns of bone quality and morphology following MRgFUS ablation. As new osseous indications for MRgFUS emerge, precise control of the post-procedural bone remodeling will be of considerable importance. For example, for an aggressive osteolytic bone metastasis, the stimulation of new bone formation might help to improve structural integrity and decrease the risk of pathologic fracture. In contrast, for a small osseous lesion in a pediatric patient, such new bone formation may be non-desirable. While prior μCT analyses in a rat model of bone focused ultrasound revealed no significant difference in a variety of mechanical properties (elastic stiffness, ultimate load, and yield load) in areas of bone remodeling, further studies are need to more completely understand the long term impact on biomechanical properties [23]. Precise control over new bone formation may also allow for novel indications such as adjuvant treatment of fracture non-union. However, without a continued improved understanding of bone microstructure and bone quality from subsequent studies, such translational efforts may be misguided.

This exploratory study was limited by its small sample size and the ablation of normal bone. Patterns of bone remodeling following

MRgFUS of diseased bone may differ significantly. Additionally, the femurs of these animals were still actively growing which may have affected the observed response. An additional limitation is that the high energy sonications were only performed at the distal ablations and low energy sonications reserved for the proximal ablations. Although the target distal and proximal regions of bone had similar appearances, location in addition to dose may have affected the process of remodeling. Another limitation of this study is that FTIR specimens were only available for half of the samples. A subsequent lack of statistical power might have limited our abilities to detect significant differences between treated and control specimens at each of the 3 and 6 week time points. Additionally, only female pigs were studied, and additional studies are needed to determine if sex may affect the osseous response to MRgFUS. Finally, FTIR specimens represent only a sampling of the targeted regions of MRgFUS ablation or contralateral control regions, and sampling may not be representative of the region as a whole.

5. Conclusions

In conclusion, in this study HR-pQCT imaging and FTIR spectroscopic analysis was used to characterize changes in bone quality and microstructure following MRgFUS ablation of normal bone in a swine model. High energy ablations demonstrated significantly increased volume of extra-cortical new bone formation following the procedure and low energy zones demonstrated increased cortical thickness. Both high and low energy ablations demonstrated lower BMD and TMD.

Acknowledgments

This publication was supported by the National Institutes of Health (NIBIB T32 training grant 1 T32 EB001631) and University of California San Francisco Department of Radiology and Biomedical Imaging Seed Grant Program.

Funding

This study was supported by the National Institutes of Health (NIBIB T32 training grant 1 T32 EB001631) and University of California San Francisco Department of Radiology and Biomedical Imaging Seed Grant Program.

Declarations of interest

All authors declare that they have no conflict of interest in relation to this work.

References

[1] R. Catane, A. Beck, Y. Inbar, T. Rabin, N. Shabshin, S. Hengst, et al., MR-guided focused ultrasound surgery (MRgFUS) for the palliation of pain in patients with bone metastases—preliminary clinical experience, Ann. Oncol. 18 (2007) 163–167, https://doi.org/10.1093/annonc/mdl335.

[2] F.A. Jolesz, N. McDannold, Current status and future potential of MRI-guided focused ultrasound surgery, J. Magn. Reson. Imaging 27 (2005) 391–399, https://doi.org/10.1002/jmri.21261.

[3] B. Liberman, D. Gianfelice, Y. Inbar, A. Beck, T. Rabin, N. Shabshin, et al., Pain palliation in patients with bone metastases using MR-guided focused ultrasound surgery: a multicenter study, Ann. Surg. Oncol. 16 (2009) 140–146, https://doi.org/10.1245/s10434-008-0011-2.

[4] A. Napoli, M. Anzidei, F. Ciolina, E. Marotta, B. Cavallo Marincola, G. Brachetti, et al., MR-guided high-intensity focused ultrasound: current status of an emerging technology, Cardiovasc. Intervent. Radiol. 36 (2013) 1190–1203, https://doi.org/10.1007/s00270-013-0592-4.

[5] E.M. Weeks, M.W. Platt, W. Gedroyc, MRI-guided focused ultrasound (MRgFUS) to treat facet joint osteoarthritis low back pain — case series of an innovative new technique — Springer, Eur. Radiol. 22 (12) (2012) 2822–2835.

[6] F. Arrigoni, A. Barile, L. Zugaro, A. Splendiani, E. Di Cesare, F. Caranci, et al., Intra-articular benign bone lesions treated with Magnetic Resonance-guided Focused Ultrasound (MRgFUS): imaging follow-up and clinical results, Med. Oncol. 34 (2017) 55, https://doi.org/10.1007/s12032-017-0904-7.

[7] D. Gianfelice, C. Gupta, W. Kucharczyk, P. Bret, D. Havill, M. Clemons, Palliative treatment of painful bone metastases with MR imaging—guided focused ultrasound, Radiology 249 (2008) 355–363, https://doi.org/10.1148/radiol.2491071523.

[8] M.D. Bucknor, V. Rieke, Y. Seo, A.E. Horvai, R.A. Hawkins, S. Majumdar, et al., Bone remodeling after MR imaging-guided high-intensity focused ultrasound ablation: evaluation with MR imaging, CT, $Na^{18}F$-PET, and histopathologic examination in a swine model, Radiology 132605 (2014), https://doi.org/10.1148/radiol.14132605.

[9] M.D. Bucknor, V. Rieke, L. Do, S. Majumdar, T.M. Link, M. Saeed, MRI-guided high-intensity focused ultrasound ablation of bone: evaluation of acute findings with MR and CT imaging in a swine model, J. Magn. Reson. Imaging 40 (2014) 1174–1180, https://doi.org/10.1002/jmri.24451.

[10] M.D. Bucknor, E. Ozhinsky, R. Shah, R. Krug, V. Rieke, Effect of sonication duration and power on ablation depth during MR-guided focused ultrasound of bone, J. Magn. Reson. Imaging 46 (2017) 1418–1422, https://doi.org/10.1002/jmri.25676.

[11] J.W. Busse, J. Kaur, B. Mollon, M. Bhandari, P. Tornetta, H.J. Schünemann, et al., Low intensity pulsed ultrasonography for fractures: systematic review of randomised controlled trials, BMJ 338 (2009) b351.

[12] J.D. Heckman, J.P. Ryaby, J. McCabe, J.J. Frey, R.F. Kilcoyne, Acceleration of tibial fracture-healing by non-invasive, low-intensity pulsed ultrasound, J. Bone Joint Surg. Am. 76 (1994) 26–34.

[13] N.M. Pounder, A.J. Harrison, Low intensity pulsed ultrasound for fracture healing: a review of the clinical evidence and the associated biological mechanism of action, Ultrasonics 48 (2008) 330–338, https://doi.org/10.1016/j.ultras.2008.02.005.

[14] G.J. Kazakia, B. Hyun, A.J. Burghardt, R. Krug, D.C. Newitt, A.E. de Papp, et al., In vivo determination of bone structure in postmenopausal women: a comparison of HR-pQCT and high-field MR imaging, J. Bone Miner. Res. 23 (2008) 463–474, https://doi.org/10.1359/jbmr.071116.

[15] H.R. Buie, G.M. Campbell, R.J. Klinck, J.A. MacNeil, S.K. Boyd, Automatic segmentation of cortical and trabecular compartments based on a dual threshold technique for in vivo micro-CT bone analysis, Bone 41 (2007) 505–515, https://doi.org/10.1016/j.bone.2007.07.007.

[16] A.J. Burghardt, H.R. Buie, A. Laib, S. Majumdar, S.K. Boyd, Reproducibility of direct quantitative measures of cortical bone microarchitecture of the distal radius and tibia by HR-pQCT, Bone 47 (2010) 519–528, https://doi.org/10.1016/j.bone.2010.05.034.

[17] J.A. MacNeil, S.K. Boyd, Accuracy of high-resolution peripheral quantitative computed tomography for measurement of bone quality, Med. Eng. Phys. 29 (2007) 1096–1105, https://doi.org/10.1016/j.medengphy.2006.11.002.

[18] A.L. Boskey, R. Mendelsohn, Infrared spectroscopic characterization of mineralized tissues, Vib. Spectrosc. 38 (2005) 107–114, https://doi.org/10.1016/j.vibspec.2005.02.015.

[19] L.M. Miller, V. Vairavamurthy, M.R. Chance, R. Mendelsohn, E.P. Paschalis, F. Betts, et al., In situ analysis of mineral content and crystallinity in bone using infrared micro-spectroscopy of the nu(4) PO_4^{3-} vibration, Biochim. Biophys. Acta 1527 (2001) 11–19.

[20] G.J. Kazakia, D. Speer, S. Shanbhag, S. Majumdar, B.R. Conklin, R.A. Nissenson, et al., Mineral composition is altered by osteoblast expression of an engineered G(s)-coupled receptor, Calcif. Tissue Int. 89 (2011) 10–20, https://doi.org/10.1007/s00223-011-9487-z.

[21] A.J. Burghardt, G.J. Kazakia, S. Majumdar, A local adaptive threshold strategy for high resolution peripheral quantitative computed tomography of trabecular bone, Ann. Biomed. Eng. 35 (2007) 1678–1686, https://doi.org/10.1007/s10439-007-9344-4.

[22] K. Kumagai, R. Takeuchi, H. Ishikawa, Y. Yamaguchi, T. Fujisawa, T. Kuniya, et al., Low-intensity pulsed ultrasound accelerates fracture healing by stimulation of recruitment of both local and circulating osteogenic progenitors, J. Orthop. Res. (2012), https://doi.org/10.1002/jor.22103.

[23] S.Y. Yeo, A. Moreno, Effects of magnetic resonance-guided high-intensity focused ultrasound ablation on bone mechanical properties and modeling, J. Ther. Ultrasound 3 (13) (2015) 1–10.